ACS OMEGA

Article

Cite This: ACS Omega 2019, 4, 19863−19874

http://pubs.acs.org/journal/acsodf

Effect of Electron-Acceptor Content on the Efficiency of Regioregular Double-Cable Thiophene Copolymers in Single-Material Organic Solar Cells

Massimiliano Lanzi*,† and Filippo Pierini‡

†Department of Industrial Chemistry "Toso Montanari", Alma Mater Studiorum-University of Bologna, Bologna 40136, Italy

‡Department of Biosystems and Soft Matter, Institute of Fundamental Technological Research, Polish Academy of Sciences, Warsaw 02-106, Poland

Supporting Information

ABSTRACT: Three regioregular thiophenic copolymers, characterized by a bromine atom or a C_{60}-fullerene group at different molar ratios at the end of a decamethylenic plastifying side chain, have been successfully synthesized using a straightforward postpolymerization functionalization procedure based on a Grignard coupling reaction. Owing to their good solubility in common organic solvents, the products were fully characterized using chromatographic, spectroscopic, thermal, and morphological techniques and used as single materials in the photoactive layers of organic solar cells. The photoconversion efficiencies obtained with copolymers were compared with those of a reference cell prepared using a physical blend of the precursor homopolymer and [6,6]-phenyl-C_{61}-butyric acid methyl ester. The best results were obtained with COP2, the copolymer with a 21% molar content of C_{60}-functionalized side chains. The use of the double-cable polymer made possible an enhanced control on the nanomorphology of the active blend, thus reducing phase-segregation phenomena as well as the macroscale separation between the electron-acceptor and -donor components, yielding a power conversion efficiency higher than that of the reference cell (4.05 vs 3.68%). Moreover, the presence of the halogen group was exploited for the photo-cross-linking of the active layer immediately after the thermal annealing procedure. The cross-linked samples showed an increased stability over time, leading to good efficiencies even after 120 h of accelerated aging: this was a key feature for the widespread practical applicability of the prepared devices.

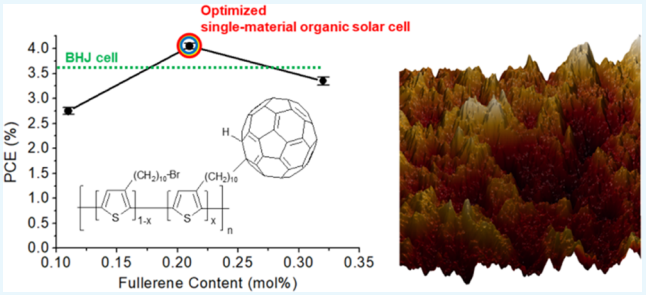

INTRODUCTION

Organic solar cells (OSCs) have attracted significant attention as a valuable source of renewable energy owing to their light weight, flexibility, and low production cost.[1] The processability and structural versatility of the semiconducting conjugated polymers used for photoactive layers[2] offer the possibility to prepare large-area solar cells on different substrates using simple and low-environmental-impact technologies.[3] OSCs based on regioregular poly(3-hexylthiophene) (P3HT) as an electron-donor (ED) and [6,6]-phenyl-C_{61}-butyric acid methyl ester (PCBM) as an electron-acceptor (EA) component have been widely studied and optimized, mainly acting on the morphology of the P3HT:PCBM photoactive blend.[4] Significant improvements were obtained with the bulk-heterojunction (BHJ) architecture, a microphase-separated blend of an ED-conjugated polymer and a fullerene derivative as an EA molecule, in which the generation of free charge carriers and their subsequent fast transport to the electrodes was highly promoted.[5,6] It is usually difficult, however, to obtain an optimized three-dimensional nanomorphology of the photoactive blend in a BHJ solar cell, since the final result depends on many factors, such as the polymer:PCBM ratio, the nature of the deposition solvent, regioregularity, molecular weight and polydispersity of the ED polymer, and annealing conditions of the deposited blend. At a molecular level, an ideal BHJ should be made up of an interpenetrated network of donor and acceptor materials, giving domains of dimensions comparable with the exciton diffusion length (5−20 nm on average)[7] without reducing the degree of crystallinity of the polymer, because the charge carrier mobility is strongly related to the structural order of the ED component.[8] Moreover, the optimum morphology of the blend, usually obtained by means of an annealing procedure, is not stable over time due to phase separation. Indeed, ED−EA nanosegregated phases are not thermodynamically stable and tend to evolve with time, forming EA clusters as a consequence of the relatively low T_g of polymers and the immiscibility of the two components. This disadvantage can be prevented either using high T_g conjugated polymers or by inserting photo-cross-linkable groups in the polymer side chains, as they can stabilize the blend

Received: August 29, 2019
Accepted: October 21, 2019
Published: November 12, 2019

DOI: 10.1021/acsomega.9b02790
ACS Omega 2019, 4, 19863−19874

Scheme 1. Synthesis of COP Copolymers

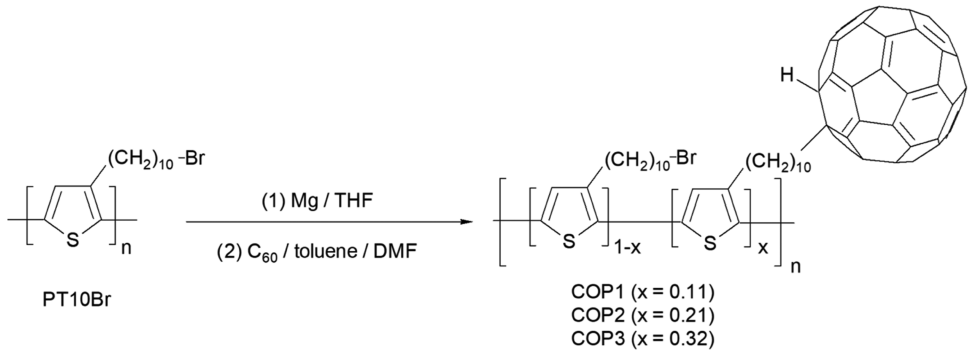

morphology after the annealing process. In the latter case, photosensitive groups should be placed at a proper distance from the polymer main chain (usually 6−10 methylene groups) to avoid any effect on the electronic properties of the conjugated backbone.[9,10] The presence of flexible alkyl side chains can also have positive effects on the solubility and morphology of "double-cable" polymers, in which the EA group is located in pendant side chains linked to the ED-conjugated backbone.[11−14] In these systems, the presence of longer alkyl spacers in side chains can induce a better nanophase separation between the polymer backbone and EA units, also improving the crystallinity of the polymer by generating an enhanced $\pi-\pi$ stacking of macromolecular chains.[15] Once again, these results evidence the importance of the morphology of the ED−EA blend, which is strongly related to the molecular design of the polymeric system used. The aim of this work is to improve the nanophase separation of some new double-cable thiophenic copolymers (COPs) to enhance their long-term performance in OSCs. The decamethylenic side chains of the synthesized thiophenic copolymers have been functionalized with a C_{60}-fullerene and a photo-cross-linkable bromine group at different molar ratios. The proposed structure is particularly intriguing since a single polymeric chain is able to carry electrons and positive holes while, at the same time, offering the possibility to chemically freeze the optimized nanophase separation obtained after the thermal annealing procedure, using a simple photo-cross-linking reaction. Therefore, the creation of a single-component photoactive blend to achieve high-performance OSCs with longer over-time stability seems to present a real challenge. The homopolymeric poly[3-(10-bromodecyl)thiophene] precursor (PT10Br, Scheme 1) was synthesized using a regiospecific polymerization procedure and then functionalized with different amounts of fullerene. The obtained copolymers (COPs, Scheme 1) were completely soluble in tetrahydrofuran (THF) and chlorinated solvents and were fully characterized using chemical and spectroscopic techniques. The molecular arrangement of COPs films was examined by atomic force microscopy (AFM) and scanning electron microscopy (SEM), whereas the effects of fullerene content on the power conversion efficiency (PCE) of the OSCs, prepared using COPs as single-material components of the photoactive layer, were evaluated. Finally, the over-time stability of the best-performing photo-cross-linked cells was compared with the uncross-linked counterparts.

RESULTS AND DISCUSSION

The architecture of a polymer-based OSC is made up of mainly three different layers: a transparent anode (usually a thin layer of indium tin oxide (ITO) evaporated on a glass slide or on a poly(ethylene terephthalate) foil); an active layer, where optical absorption and charge generation take place; and a cathode of an evaporated metal (typically Al). When a photon is absorbed by the active layer, which is essentially made up of a physical blend of an electron-donor (ED) and -acceptor (EA) material, it leads to the generation of an exciton, which is a Coulombically bound electron−hole pair. The energy offset between the frontier molecular orbitals of the donor and acceptor should then provide the driving force necessary for the exciton dissociation to free charge carriers (i.e., an electron and a positive hole), but this process is usually hindered by the short lifetime of the exciton. Indeed, in polymeric heterojunctions, exciton dissociation takes place at the ED−EA interface and only excitons generated at a distance shorter than their diffusion length are capable of producing free charge carriers. In this context, the morphology of the active blend plays a fundamental role because ED and EA components usually suffer from marked phase separation, due to their immiscibility,[5] when only homogeneous and interpenetrated blends can effectively increase the number of dissociated excitons, with positive effects on the efficiency of the solar cell.

In this work, we report on the synthesis of a regioregular copolymer in which the EA moiety (C_{60} fullerene) is covalently linked in the side chain of a polythiophenic ED-conjugated backbone. Since the proximity of the donor and acceptor units could lead to charge recombination phenomena,[16] we chose a length of 10 methylenic units for the oligomethylenic spacer between ED and EA groups. It is worth mentioning that the choice of the most suitable spacer length is indeed very difficult; on the one hand, if the alkylic spacer is too long, the glass-transition temperature of the polymer can be lower than the room temperature, leading to poor filmability, whereas, on the other hand, if the spacer is too short, the final polymer can be insoluble in common organic solvents. In view of this, the right length of the oligomethylenic spacer is a delicate interbalance between thermal, physical, and morphological properties.

The synthesized copolymer is particularly promising, as a single polymeric material is able to carry electrons and positive holes (double-cable polymer). About it, recently some authors reported the synthesis of a new double-cable conjugated polymer resulting in a record efficiency of 6.3% in single-material solar cells.[17] Moreover, the proposed structure can provide a faster inter- and intrachain transport of holes, a more

DOI: 10.1021/acsomega.9b02790
ACS Omega 2019, 4, 19863−19874

Table 1. Polymer Characteristics

sample	yield[a] (%)	HT dyads[b] (%)	M_n[c] (kDa)	M_w/M_n[c]	fullerene content[d] (mol %)	polymer/C_{60} ratio[d] (w/w)
PT10Br	76	98	24	1.22	0	1:0.00
COP1	77	96	30	1.23	11	1:0.27
COP2	71	96	35	1.25	21	1:0.53
COP3	66	96	40	1.25	32	1:0.83

[a]In a fractionated polymer. [b]Regioregularity from ^{1}H NMR expressed as head-to-tail dyad percentage. [c]Determined by gel permeation chromatography (GPC) relative to polystyrene standards. [d]Determined by ^{1}H NMR.

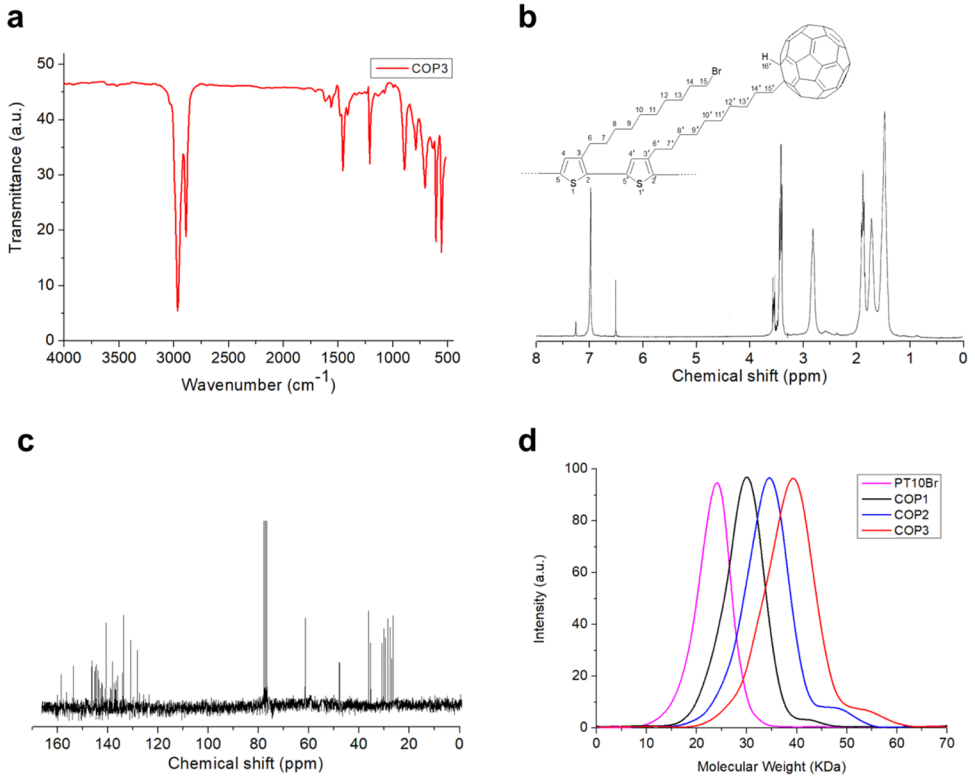

Figure 1. Copolymer chemical structure. (a) FT-IR spectrum of COP3 as a film on a Ge disk (cast from $CHCl_3$ solution). (b) ^{1}H NMR spectrum of COP3 in $CDCl_3$ and atom numbering for COPs. (c) ^{13}C NMR of COP3 in $CDCl_3$. (d) GPC eluograms of the synthesized polymers.

effective displacement of electrons along fullerenes, and a higher interfacial area between the donor and the acceptor because segregation phenomena are strongly limited. Basically, we prepared and characterized three copolymer samples having a different fullerene content, to evaluate the effect of EA concentration on the power conversion efficiency of the device. The use of the postpolymerization approach has been effective, facilitating the synthetic procedures required for the obtainment of polymers with the desired amount of functional groups.[18]

Synthesis and Characterization of Copolymers. The general procedure for the preparation of copolymers is shown in Scheme 1. The precursor homopolymer PT10Br was obtained by means of a regiospecific procedure, namely, the Grignard metathesis (GRIM) polymerization, involving the cross-coupling of the organomagnesium intermediate prepared by reacting 2,5-dibromo-3-(10-bromodecyl)thiophene (2,5BT10Br) with a preformed Grignard reactive (CH_3MgCl) in the presence of the $NiDPPPCl_2$ catalyst. Its characteristics are shown in Table 1. PT10Br was then dissolved in anhydrous THF and added with Mg turnings to obtain the corresponding ω-bromomagnesium derivative, which was directly reacted with a solution of fullerene in toluene. *N*,*N*-Dimethylformamide (DMF) was also added to the reaction mixture since the presence of polar additives can improve the coupling reaction yield. Indeed, Matsuo et al.[19] reported that polar solvents are able to enhance the nucleophilicity of the Grignard reagent while stabilizing the Mg intermediate.

The obtained copolymers proved to be soluble in the tested solvents ($CHCl_3$, CH_2Cl_2, CB, and THF) up to 30 mg mL^{-1} (COP1 and COP2) and 15 mg mL^{-1} (COP3). However, a large amount of insoluble fractions was observed when the fullerene content was further increased during preliminary trials.

The Fourier-transform infrared (FT-IR) spectrum of the copolymer COP3 is shown as an example in Figure 1a. The presence of evident absorptions at 1429, 1174, 577, and 526 cm^{-1}, which can be ascribed to C_{60} fullerene,[20] confirms the expected substitution in side chains.

The ^{1}H NMR and ^{13}C NMR spectra of COP3 are shown in Figure 1b,c, respectively. The spectra of COP1 and COP2 are very similar to those reported before. The ^{1}H NMR spectrum shows two signals in the aromatic region, at 7.01 and 6.45 ppm, which can be ascribed to the H-4 thiophenic proton and to the proton directly attached to the fullerene group, respectively. The signals at 3.58 and 3.42 ppm can be ascribed to

DOI: 10.1021/acsomega.9b02790
ACS Omega 2019, 4, 19863−19874

methylenic protons α^- to C_{60} and Br group, respectively, whereas the ratio between their relative intensities gives the fullerene content of the copolymer (32% molar ratio, 1:0.83 polymer/C_{60} weight ratio). The resonance of methylenic protons α^- to the thiophene ring is split into two signals at 2.83 and 2.58 ppm, which are ascribable to the dyads originating from different monomer couplings: the peak at the lower fields can be assigned to head-to-tail (HT) junctions, whereas that at the higher fields to head-to-head and tail-to-tail (HH, TT) junctions.[21] The regioregularity degree is given by the ratio of their integrated intensities (96% HT), in good agreement with the values usually reported for GRIM polymerization of alkylthiophene monomers.[22] Finally, the remaining signals at a higher field can be attributed to the central methylenes of the side chains.

As detailed in Experimental Section, the ^{13}C NMR spectrum of COP3 (Figure 1c) shows the expected signals ascribable to the 3-(10-bromodecyl)thiophene and 3-(10-fullerenyldecyl)-thiophene units. Moreover, the prevalence of only four evident signals ascribable to the thiophenic carbons (at 139.21, 133.95, 129.71, and 127.93 ppm) further confirms the prevalence of one kind of configurational sequence (HT−HT) in the copolymer structure, as already observed by ^1H NMR analysis.

The gel permeation chromatography (GPC) of the precursor polymer and of the three fullerene-attached copolymers produced the traces shown in Figure 1d. The small shoulder of the copolymers peaks at higher molecular weights, which was not detected for the PT10Br sample, may be ascribed to a small amount of aggregates or cross-linked products.[23] Moreover, the GPC analysis shows the effectiveness of the purification procedure adopted for the COP samples since any evident peak was detected at around 27.8 min, corresponding to C_{60}-fullerene elution time in the conditions used (Figure S1).

Spectroscopic Properties. Figure 2a shows the absorption spectra of copolymers and of the physical blend PT10Br/PCBM 1:1 w/w, shown for comparison, in $CHCl_3$ solutions. We have chosen this weight ratio for the reference blend since it represents the optimal composition for the commonly used P3HT:PCBM BHJ solar cells.[24] Spectra were normalized at 264 nm, corresponding to the main absorbance of C_{60} fullerene.[25]

The absorption at 452 nm (455 nm for COP2) may be ascribed to the polythiophenic component and corresponds to the average conjugation length of seven thiophenic rings.[26] Moreover, the absorptions at this wavelength decrease with the fullerene content, following a trend similar to that determined by ^1H NMR analysis.

A similar result can be obtained when observing the UV−vis spectra of thin films cast by the doctor blade technique (Figure 2b). This time, however, the behavior of the polythiophenic component was quite different from the previous case. Indeed, the absorption of the conjugated backbone was strongly red-shifted compared to that in solution: up to 547 nm for the blend, 536 nm for COP1, 535 nm for COP2, and 533 nm for COP3, corresponding to a mean conjugation length of 21 for PT10Br/PCBM and of around 17 conjugated thiophenes for COP samples. These values can be obtained using the semiempirical relation found by Jiang,[27] which relates the length of the conjugated π-electron structure n_L with the wavenumber of the absorption peak of the UV−vis spectrum

$$\nu = A - B(1/2)^{2/n_L}$$

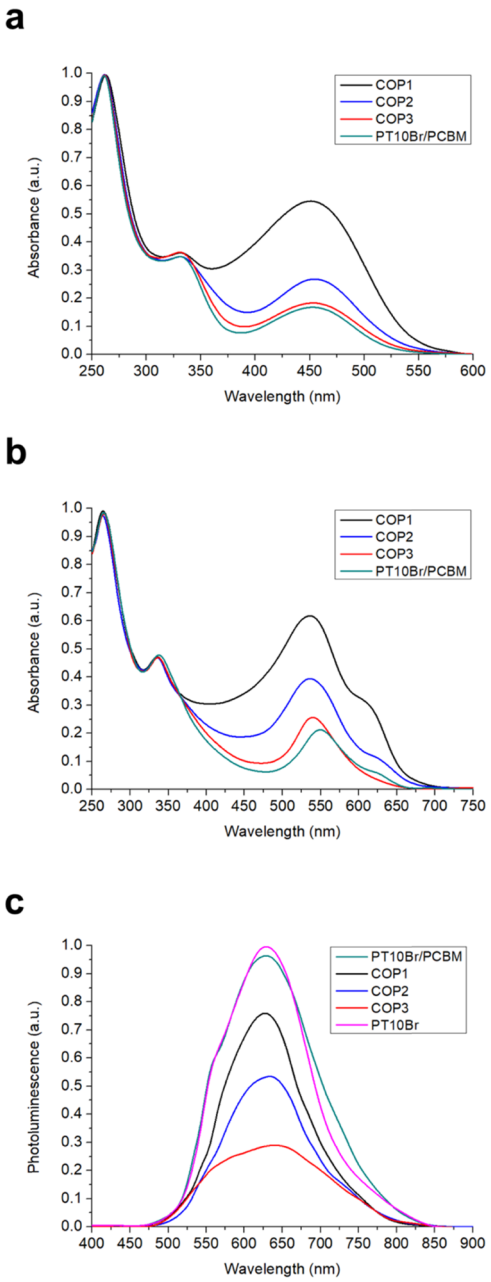

Figure 2. Spectroscopic properties. (a) UV−vis absorption spectra of copolymers and the PT10Br/PCBM blend in $CHCl_3$ (spectra have been normalized at 264 nm). (b) UV−vis absorption spectra of copolymers and of the PT10Br/PCBM blend in a film on quartz slides (spectra have been normalized at 264 nm). (c) Photoluminescence (PL) spectra of PT10Br, the PT10Br/PCBM blend, and copolymers in $CHCl_3$ (excitation wavelength: 450 nm).

where A and B are constants determined for the different conjugated polymers.

Furthermore, the presence of an evident shoulder at around 600 nm, ascribable to the 0−0 pure electronic transition (E_{0-0}), indicates the existence of crystalline domains in the polymers since this absorption is evident only in conformational ordered polythiophenic chains, which are able to form interchain $\pi-\pi$ stacking in the solid state.[28] The relative intensity of the E_{0-0} transition is particularly evident in COP1, COP2, and PT10Br/PCBM blend spectra, whereas it is less evident in the COP3 sample. The results obtained suggest that

DOI: 10.1021/acsomega.9b02790
ACS Omega 2019, 4, 19863−19874

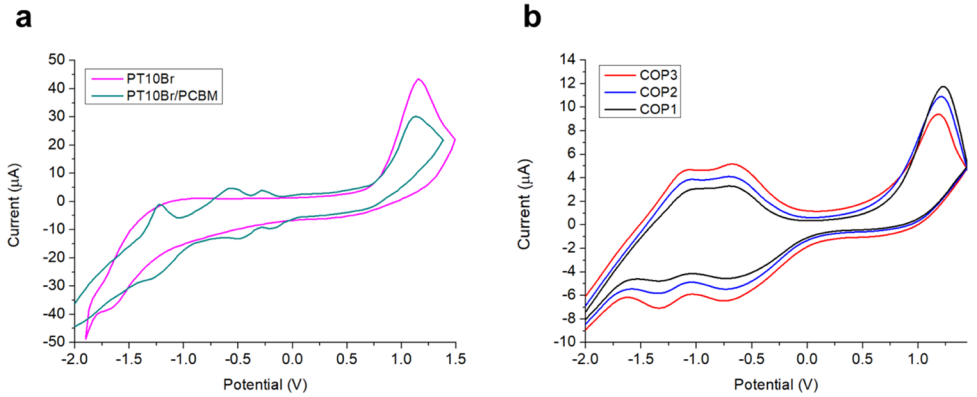

Figure 3. Electrochemical characterization. CV curves recorded in a 0.1 M $TBAPF_6$/acetonitrile solution at 0.05 V s^{-1} for a Pt electrode coated with (a) PT10Br and PT10Br/PCBM; (b) three synthesized COP samples.

Table 2. Electrochemical Properties of the Polymer Films

polymer	E_{ox} (V)	E_{HOMO} (eV)	$E_{LUMO,opt}$ (eV)	$E_{LUMO,ec}$ (eV)	$E_{g,opt}$ (eV)	$E_{g,ec}$ (eV)
PT10Br/PCBM	0.76	−5.16	−3.30	−3.37	1.86	1.79
COP1	0.78	−5.18	−3.30	−3.34	1.88	1.84
COP2	0.80	−5.20	−3.33	−3.36	1.87	1.84
COP3	0.80	−5.20	−3.31	−3.37	1.89	1.83

the bulky fullerene moiety, when present at high molar content (more than 21%) in a copolymer structure, can lower the degree of order of polymeric chains. Moreover, the comparison between the spectrum of the PT10Br/PCBM blend (Figure 2b) and that of PT10Br in a film (Figure S2) indicates that the fullerene-based EA molecules, also, can lower the conformational order of conjugated chains in the solid state. Indeed, the presence of PCBM causes the blue shift of the absorption maximum wavelength (from 558 to 547 nm) passing from the pure polymer to the polymer blend.

The photoluminescence (PL) spectra of copolymers, PT10Br, and the physical blend PT10Br/PCBM 1:1 w/w in $CHCl_3$ solutions at about 10^{-5} mol L^{-1} polymer concentration are shown in Figure 2c. The fluorescence spectra of PT10Br and PT10Br/PCBM blend are very similar since energy transfers from the polymer to PCBM are very low in diluted solutions. On the other hand, the photoluminescence decreases significantly in copolymers; the reduction observed, which is roughly proportional to the fullerene content, may be attributed to an efficient photoinduced charge separation between ED and EA groups,[29] facilitated by their close proximity.

Electrochemical Characterization. The homopolymer and the three copolymers were electrochemically characterized by cyclic voltammetry (CV) using a polymer-coated Pt disk as the support electrode, acetonitrile containing $TBAPF_6$ as the supporting electrolyte, Pt wire as the counter electrode, and saturated calomel electrode (SCE) as the reference electrode. The PT10Br film showed oxidation and reduction onsets at 0.77 and −1.08 V, respectively (Figure 3a). These values made it possible to directly calculate the energy of the highest occupied molecular orbital (HOMO = −5.17 eV), the lowest unoccupied molecular orbital (LUMO = −3.32 eV), and the electrochemical band gap ($E_{g,ec}$ = 1.85 eV), considering that the SCE reference electrode has a potential of 4.40 eV relative to vacuum.[30] The polymer energy gap was also determined by the onset of its UV−vis spectrum in a film (675 nm), giving a value ($E_{g,opt}$ = 1.84 eV) very close to that obtained using the electrochemical method, even if the comparison between the values obtained by different methods can be misleading, as evidenced by Bredas.[31]

The evaluation of the electrochemical parameters for copolymers and the physical blend was indeed more difficult. Indeed, since in this case the reduction peaks of the polythiophenic component were embedded with those ascribable to C_{60} fullerene (Figure 3a,b),[32] the LUMO energy values were determined indirectly, by considering the fact that they correspond to the HOMO energy and the optical energy gap evaluated from the onset of the UV−vis spectrum of the copolymer in a film.[33] We were encouraged to perform this evaluation by the very similar E_g values obtained in the case of precursor polymer PT10Br.

However, we also tried to evaluate E_g using the onset of the reduction peak at lower potential related to the fullerene moiety to calculate LUMO energy levels ($LUMO_{ec}$), obtaining the values reported in Table 2 ($E_{g,ec}$). These values are in a good agreement with those determined by means of the optical band gap ($E_{g,opt}$) even if the trend does not appear the same; this is probably due to the difficulty of assessing the exact position of the peaks in the reduction region of CV spectra.

Table 2 shows the electrochemical data of the prepared samples calculated using the optical band gap $E_{g,opt}$.

The electrochemical parameters of the copolymers and the PT10Br/PCBM physical blend are similar to those measured for PT10Br, thus suggesting that both the fullerene pendant group and the conjugated polythiophene chain retain their individual electrochemical properties. Moreover, all of the examined samples showed a HOMO-level energy, which is particularly low in comparison to the value reported for the standard reference P3HT (−4.8 eV),[34] a characteristic that is favorable for obtaining a high open-circuit voltage,[35] with potential positive implications on the conversion efficiency of the final devices.[36]

Thermal and X-ray Diffraction (XRD) Analyses. Differential scanning calorimetry (DSC) data of the examined samples are shown in Table 3.

DOI: 10.1021/acsomega.9b02790
ACS Omega 2019, 4, 19863−19874

Table 3. Glass-Transition (T_g), Melting (T_m), Crystallization (T_c), and Decomposition (T_d) Temperatures of the Synthesized Polymers

sample	T_g (°C)	T_{m1} (°C)	T_{m2} (°C)	T_c (°C)	T_d[a] (°C)
PT10Br	−11.8	47.3, 76.7	158.2	124.1	261
PT10Br/PCBM		56.4	150.9	114.2	238
COP1		41.6	156.4	123.9	249
COP2		37.7	151.5		244
COP3		36.2	149.8		233

[a]Determined by thermogravimetric analysis (TGA) in air.

The first heating run on a pristine PT10Br sample (Figure 4a) showed (i) two endothermic peaks in the 35−85 °C range ascribable to side-chain melting and (ii) a more intense endothermic transition at around 158 °C, which corresponds to the melting of the main chains. In the cooling process, a sharp exothermic peak at 124 °C can be seen, possibly due to the crystallization of the polymer melt.[37,38] An evident second-order transition (T_g) can also be seen at around 12 °C. When the homopolymer is blended with PCBM, the melting and crystallization peaks become less evident and shift to lower temperatures. The same results can be observed in copolymer thermograms at increasing fullerene content (Figure 4b), thus suggesting that the presence of the sterically hindering fullerene probably promotes the formation of less ordered and more amorphous structures. TGA thermograms, recorded in air at a heating scan of 10 °C min^{-1} (Figure 4c), showed that the thermal decomposition of the examined samples begins around 250 °C, whereas T_d values tend to decrease with the fullerene content (Table 3). These results are in line with those obtained by Kumar et al.,[39] who reported that the addition of carbon nanomaterials to P3HT reduced its thermal stability. The relatively high decomposition temperatures of all of the samples, however, make them suitable for the thermal treatments provided for the assembling of the final OSCs.

PT10Br, the PT10Br:PCBM 1:1 w/w physical blend, and fullerene-attached copolymers films were also analyzed by X-ray diffraction after the annealing procedure used for the preparation of the photovoltaic cells (120 °C, 30 min, 10^{-3} mmHg).

All of the samples show diffraction peaks at low angles (Figure 4d), ascribable to a lamellar structure usually observed in crystalline regioregular polyalkylthiophenes. The *d*-spacings of the diffraction from (100) slowly increase from 20.83 to 21.91 Å with fullerene content, and a similar trend can also be observed for the diffraction from the (010) $\pi-\pi$ stacking distance (Table 4). These results indicate that the presence of the bulky-group fullerene can effectively hinder the crystalline packing of the thiophenic component of the polymers, as already suggested by thermal analysis, but not to the point where the crystallization becomes impossible. It is interesting to note that the physical blend shows larger and less intense peaks when compared to copolymer patterns, as well as longer in-plane and stacking distances, thus indicating a decreased structural order and macromolecules packing in the PT10Br/PCBM sample.

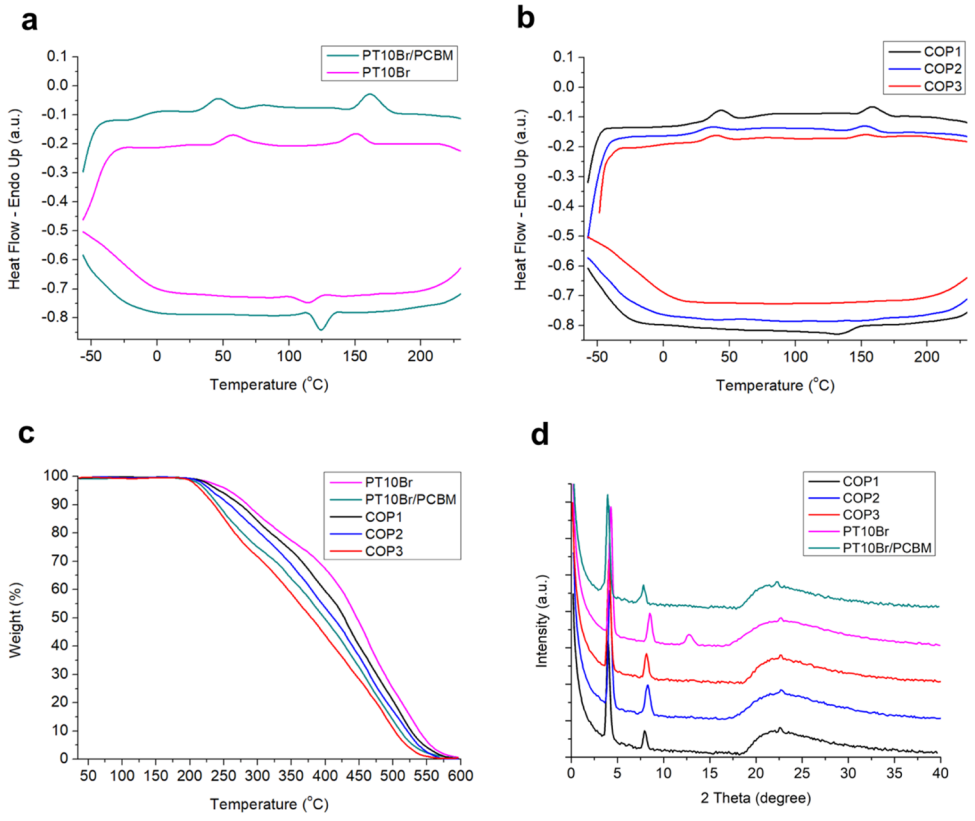

Figure 4. Structural properties of polymers. (a) DSC thermograms (first run) of PT10Br and the PT10Br/PCBM physical blend recorded under nitrogen at a scan speed of 5 °C min^{-1}. (b) DSC thermograms of COP samples. The upper lines were obtained from heating scans, whereas the lower lines came from cooling scans. (c) TGA graphs recorded in air at a 10 °C min^{-1} scan rate. (d) X-ray diffractograms of PT10Br, PT10Br/PCBM, COP1, COP2, and COP3 reported in a range of 2θ from 0 to 40°.

DOI: 10.1021/acsomega.9b02790
ACS Omega 2019, 4, 19863−19874

Table 4. Structural Parameters of the Synthesized Copolymers in a Film

sample	low-angle diffractions (2θ, degree)	high-angle diffractions (2θ, degree)	in-plane PT chain distances (Å)	planes stacking distances (Å)
PT10Br	4.24; 8.51; 12.79	22.66	20.83	3.92
PT10Br/PCBM	3.95; 7.98	22.15	22.35	4.01
COP1	4.19; 8.41	22.55	21.05	3.94
COP2	4.07; 8.19	22.49	21.67	3.95
COP3	4.03; 8.11	22.38	21.91	3.97

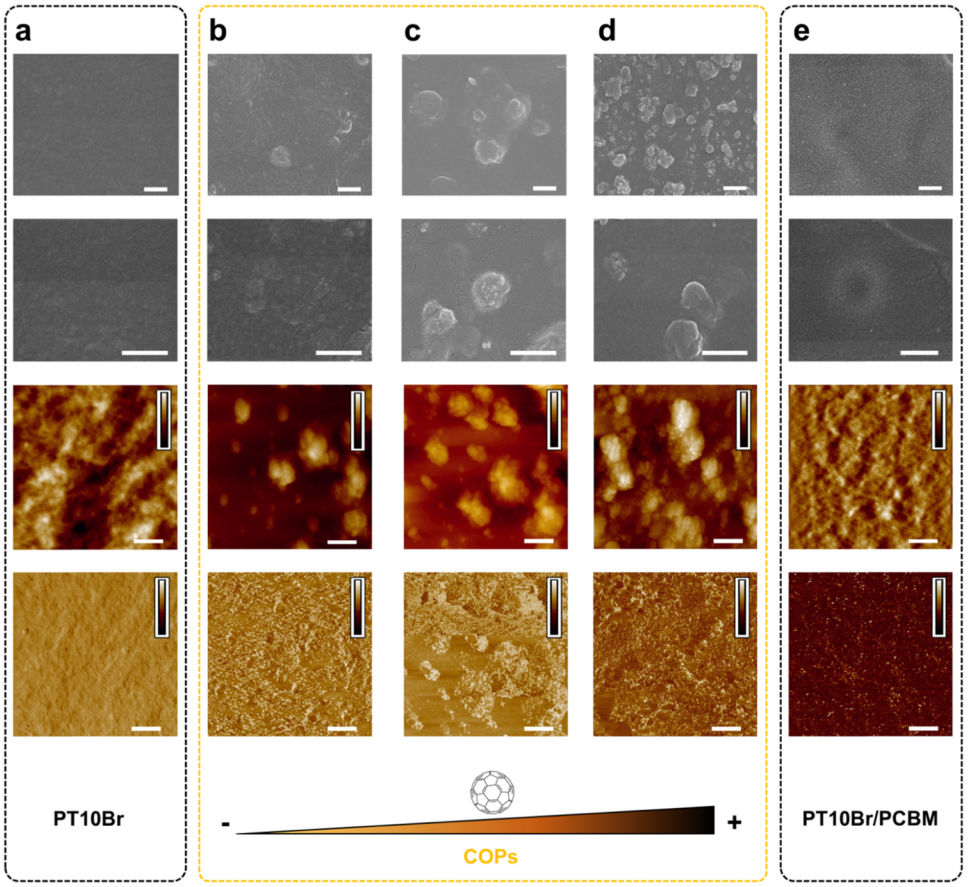

Figure 5. Active layer surface structure of organic solar cells. FE-SEM (at two different magnifications) and AFM topographical and phase images of the active material layers obtained from (a) PT10Br, (b) COP1, (c) COP2, (d) COP3, and (e) PT10Br/PCBM. All of the AFM and FE-SEM scale bars are equal to 500 nm. The AFM image z-scales are equal to (a) 7 nm and 5°, (b) 35 nm and 40°, (c) 45 nm and 40°, (d) 60 nm and 70°, and (e) 10 nm and 30°.

Morphological Characterizations. Both atomic force microscopy (AFM) and field emission scanning electron microscopy (FE-SEM) were used to investigate the effects of material chemical composition and fullerene content in the polythiophene copolymers on the nano- and microstructure of the organic solar cells (Figure 5). Figure 5a shows the morphology of an active layer made by PT10Br. As is evident by observing the FE-SEM images as well as the AFM topography, the material is extremely flat and does not present any typical morphological features. Additionally, the AFM phase image confirms the uniformity of the sample structure and the absence of phase separation. The effect of the copolymer fullerene content on the nano- and microstructuration of the single-material double-cable layer (Figure 5b–d) reveals the significance of the chemical structure optimization in fabricating well-developed polymer structures and, in turn, enhancing the solar cell efficiency. The thin-film morphology of single-material active layers made up by COP1, COP2, and COP3 was significantly affected by the relative concentration of the fullerene-bearing monomer in the copolymer chain. The COP1 thin film showed a relatively smooth surface compared to other copolymer-based materials, but it was rougher than the PT10Br layer. SEM images shown in Figure 5b highlighted a low number of microsized features, whereas AFM images demonstrated the presence of the typical double-cable polymer nanostructuration. As can be seen in Figure 5c, the increase in fullerene concentration affected the microstructure of the active layer, which became more evident, whereas the nanostructure remained stable even though the copolymer reached a molar content of C_{60}-functionalized side chains of 21%, as in the case of COP2. When the concentration of a bulky group such as a fullerene became very high (COP3, Figure 5d), both the micro- and nanostructures were affected by the aggregation tendency of the fullerene. The microscale structure was completely dominated by the presence of large aggregates; most importantly, even the nanoscale phase separation (which is of main importance to achieve satisfactory efficiencies) was affected by the presence of C_{60} fullerene, thus

DOI: 10.1021/acsomega.9b02790
ACS Omega 2019, 4, 19863−19874

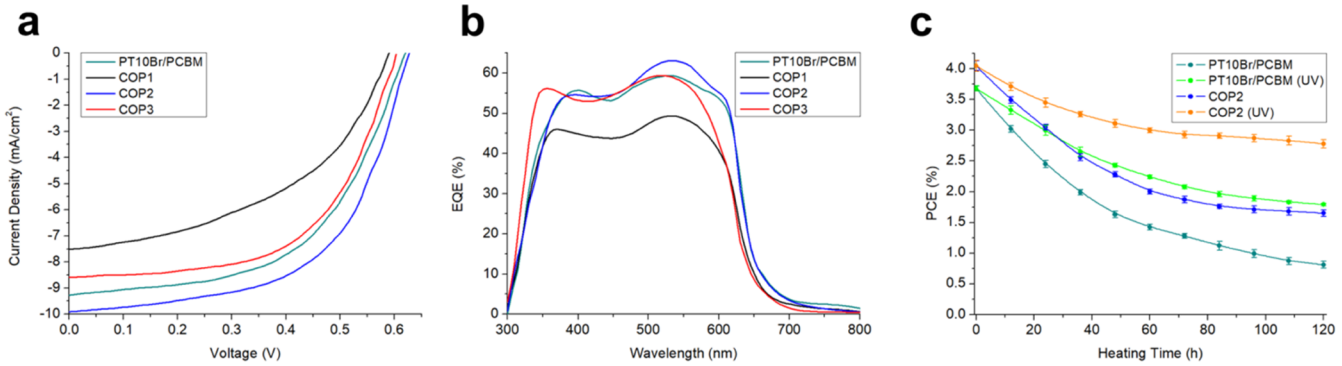

Figure 6. Solar cell performance. (a) Current density−voltage (J−V) characteristics for the best-performing cells under AM 1.5 1 sun illumination. (b) External quantum efficiency (EQE) spectra of organic solar cells fabricated using a thin layer of COP1, COP2, COP3, and PT10Br/PCBM blend films in the active material. (c) Efficiency of OSCs heated at 150 °C over time (the devices were prepared under the same experimental conditions and UV samples were exposed to UV light for 30 min).

Table 5. Photovoltaic Characteristics of the Devices Obtained

sample	J_{sc} (mA cm^{-2})[a]	V_{oc} (V)[a]	FF[a]	PCE (%)[a]
PT10Br/PCBM	9.46 ± 1.2	0.61 ± 0.01	0.64 ± 0.02	3.68 ± 0.05
COP1	7.77 ± 1.3	0.59 ± 0.01	0.60 ± 0.05	2.75 ± 0.07
COP2	9.91 ± 1.2	0.62 ± 0.01	0.65 ± 0.04	4.05 ± 0.06
COP3	8.86 ± 1.1	0.60 ± 0.01	0.62 ± 0.03	3.35 ± 0.08

[a]Average values collected from 10 devices.

confirming the previous results obtained by DSC and XRD. Finally, the developed copolymer materials were compared with a typical BHJ active material produced by a physical PT10Br/PCBM blend (Figure 5e). The inclusion of PCBM led to increased roughness compared to the pure material layer shown in Figure 5a, mainly due to the formation of the typical BHJ nanoscale phase separation.

Solar Cell Fabrication and Performance. A series of OSCs with the structure ITO (80 nm)/PEDOT:PSS (100 nm)/photoactive polymer (150 nm)/Al (50 nm) were prepared under the conditions described in Experimental Section, with the aim of comparing the performance of copolymers, used as single materials, with that of the physical blend (PT10Br/PCBM). Current density−voltage curves of the devices are shown in Figure 6a, whereas the key photovoltaic parameters (short-circuit current density J_{sc}, open-circuit voltage V_{OC}, fill factor FF, and power conversion efficiency PCE) are summarized in Table 5. The reported data are the result of the measurement of 10 devices for each sample prepared under the same operative conditions. The device with the copolymer at 21% molar fullerene content (COP2) showed the highest PCE value, whereas the presence of a lower (COP1) or a higher (COP3) EA content in the copolymer structure produced worse results. Therefore, with a low fullerene amount, most likely, the ED/EA components are not able to form percolation channels for the charge transport to the electrodes.[40,41] Indeed, even if COP1 shows an intense absorption in the visible range (Figure 2b), its low performance could be related to a lower degree of exciton dissociation at the ED/EA interfaces and to a less efficient transport of the electrons to the cathode, determined by the low amount of EA molecules. The COP1 sample shows the lowest value of photocurrent (Table 5), and this fact is in agreement with the results reported by Durrant et al.,[42] which observed that the J_{sc} value usually increases with the increasing EA content. On the other hand, excessively high concentrations of a fullerene can lead to aggregation phenomena and hence to poor charge separation and electron/hole recombination. In this context, it must be emphasized that COP2 showed a PCE higher than that of the reference PT10Br/PCBM physical blend, suggesting the attainment of an optimized morphology of the photoactive film layer prepared with this single-material copolymer.

External quantum efficiency (EQE) spectra of the devices are compared in Figure 6b. Spectral profiles were very similar, revealing a remarkable photocurrent response over the absorption range 300−620 nm, with the exception of the COP1 sample. The solar cell photocurrent densities (J_{sc}), calculated by integrating EQE spectra with the AM 1.5 G spectrum,[43] were 7.23, 9.28, and 8.34 mA cm^{-2} for COP1, COP2, and COP3, respectively, and 9.12 mA cm^{-2} for the PT10Br/PCBM blend. The J_{sc} values calculated from EQE spectra are very consistent with those derived from J−V curves.

Solar Cell Stability. The morphology of polymer−fullerene layers should be effectively controlled not only during the film formation but also when the device is tested or used for its features. Usually, the thermal annealing procedure is the first step toward optimizing the nanomorphology of the photoactive layer.[44] Indeed, heating the active layer of the organic photovoltaics (OPV) cell makes it possible for polymer chains to reorganize in a more crystalline structure and for the fullerene molecules to diffuse into the blend and reorder in a thermodynamically more favorable way. Annealing generally results in higher photon-to-charge conversion at all wavelengths across the polymer blend absorption spectrum and also in an enhanced mobility of the charge carriers.[45] However, the obtained bicontinuous network with nanometer-scale phase segregation is not thermally stable over time since the polymer−fullerene nanoclusters are intrinsically thermodynamically unstable, as they are created by kinetically trapping electron-donor/acceptor nanostructures. Consequently, with the light exposure of the final devices (or in the case of long

DOI: 10.1021/acsomega.9b02790
ACS Omega 2019, 4, 19863−19874

storage times), the two components spontaneously tend to segregate, producing the original macrophase separation. To enhance the phase stability of the prepared solar cells, a photo-cross-linking procedure was applied to the synthesized copolymers at room temperature by taking advantage of the presence of bromine groups in some side chains.[46,47] Photo-cross-linking was carried out on the annealed photoactive layers just before Al cathode deposition, using a Philips UV-C PL 11 W lamp (3.2 W@250 nm, λ_{max} at 253.7 nm, distance of irradiation 5 cm) with an exposure time of 30 min. The right irradiation time was determined by exposing copolymer films to UV light for different times; the exposed films were then immersed in $CHCl_3$ for 20 min, rinsed with methanol, and dried. Film weights before and after $CHCl_3$ dipping were then compared. After 30 min of UV exposure, the copolymer films were totally insoluble in the chlorinated solvent, proving the effectiveness of the cross-linking procedure.

The thermal stability was studied by submitting five samples of the better-performing OSCs (COP2 and PT10Br/PCBM) to constant heating at 150 °C under a vacuum for different times (up to 120 h) to simulate an accelerated aging (Figure 6c). Preliminary tests were performed using a regioregular sample of poly(3-decylthiophene) (PT10H) synthesized as reported in the Supporting Information, blended with PCBM (1:1 w/w). In this case, the photoconversion efficiencies decreased to 23 and 22% of the initial value for the unexposed and UV-exposed sample, respectively (Figure S3). As for PT10Br/PCBM and COP2 unexposed samples, their PCEs decreased to 22% (PT10Br/PCBM) and 41% (COP2) of the initial value after 120 h at 150 °C, thus evidencing the intrinsic higher stability of the photoactive layer consisting of a single-material double-cable copolymer, as compared to the conventional polymer/PCBM blend architecture. The covalent linkage of the EA moiety to the ED-polymer structure has a beneficial impact on the time and thermal properties of the final device by reducing the mobility of the two components. The effectiveness of the photo-cross-linking procedure is proven by the results obtained with the UV-exposed samples, showing very stable device performances even after 120 h of annealing at 150 °C (49 and 69% of the initial device efficiency for the physical blend and the copolymer, respectively). The results obtained clearly evidence that the photo-cross-linking procedure is a fast and effective method for enhancing the thermal stability of OSCs.

CONCLUSIONS

In this paper, we reported on the synthesis of three regioregular photo-cross-linkable thiophene copolymers with different electron-acceptor contents, with the aim of preparing high-performance single-component organic photovoltaic solar cells. The new double-cable donor−acceptor polythiophene derivatives have been successfully synthesized using an easy and effective postpolymerization approach on poly[3-(10-bromodecylthiophene)] (PT10Br) by means of a Grignard coupling reaction with C_{60} fullerene. The precursor polymer was functionalized with different amounts of the fullerene, to attain the best compromise between the solubility in common organic solvents and the photoconversion efficiency of the obtained copolymers. The soluble copolymers were characterized by GPC, FT-IR, NMR, and elemental analysis to find their fullerene content. The homopolymeric precursor was also used to prepare a physical blend with PCBM, which was used as a reference. The copolymer with the 21% molar content of the fullerene showed the best-performing properties and yielded a power conversion efficiency higher than that of the reference blend (4.05 vs 3.68%), together with a slower decrease in photoelectric properties over time. Finally, the stability of the prepared cells has been further improved by photo-cross-linking the brominated groups at the end of the side chains. The simplicity of the proposed synthetic approach, which involves straightforward reactions characterized by high yields, and the obtainment of soluble copolymers, bearing versatile functional groups inserted in the terminal position of side chains, indicate that the prepared donor−acceptor polymeric hybrids may be valuable candidates for the next generation of solution-processable single-material solar cells.

EXPERIMENTAL SECTION

Materials. Commercially available reagents from Sigma-Aldrich (Merck KGaA, Darmstadt, Germany) were used throughout without further purification unless otherwise stated; solvents (HPLC grade) were dried by standard procedures, stored over molecular sieves, and handled in a moisture-free atmosphere.

Measurements. ^1H and ^{13}C NMR spectra were recorded in $CDCl_3$ on a Varian Mercury Plus (400 MHz) spectrometer using tetramethylsilane as a reference. IR spectra were recorded on Ge or KBr disks using a PerkinElmer Spectrum One or a Bruker Alpha Platinum spectrophotometer. UV−vis spectra were recorded on a PerkinElmer Lambda 19 spectrophotometer using about 10^{-5} M polymer solutions in spectroquality solvents in Suprasil quartz cuvettes (1 cm × 1 cm) or films on quartz slides. Molecular weights were estimated by gel permeation chromatography (GPC) using $CHCl_3$ solutions on an Agilent PL-GPC 50 apparatus equipped with a μ-Styragel mixed bed column (Waters HR 4E) referenced to polystyrene standards. Elemental analysis was performed by Redox Laboratories, Italy. Fluorescence spectra were recorded on an Edinburgh FLSP 920 spectrofluorimeter using the same conditions described for UV−vis analysis. A DSC TA Instruments Q2000 was used for the thermal analysis in the −50 to 230 °C range at a rate of 5 °C min^{-1} in a nitrogen atmosphere. Thermogravimetric analyses (TGA) were performed at 10 °C min^{-1} in air using a TGA TA Instruments Q600. All electrochemical measurements were performed using an Autolab PGSTAT204 (Metrohm) potentiostat/galvanostat at a potential scan rate of 100 mV s^{-1}. The polythiophenes to be examined were deposited from chlorobenzene solutions on a Pt disk that served as the working electrode. The working electrode, counter electrode (Pt wire), and reference electrode (aqueous saturated calomel electrode) were immersed in an acetonitrile solution with tetrabutylammonium hexafluorophosphate ($TBAPF_6$, 0.1 M) as the supporting electrolyte using a one-compartment three-electrode cell.

AFM images were scanned in the tapping mode in air, using an atomic force microscope (Ntegra, NT-MD) equipped with a rectangular silicon cantilever (HA_NC, NT-MDT, nominal spring constant of 12 N m^{-1}, and tip curvature radius smaller than 10 nm). The sample size taken was 3.0 μm × 3.0 μm at a scan rate of 0.5 Hz, whereas the drive frequency of the cantilever was approximately 235 kHz. Field emission scanning electron microscopy (FE-SEM, Nova NanoSEM 450, FEI) was used at an accelerating voltage of 10 kV and a working distance of around 4 mm, to image the surface of the samples. An 8 nm thick gold layer was used for coating the samples prior to

DOI: 10.1021/acsomega.9b02790
ACS Omega 2019, 4, 19863−19874

observations. X-ray diffraction (XRD) patterns of polymer films were obtained by a Philips PW1050−PW1710 system (Cu Kα radiation).

Photovoltaic Cell Fabrication and Measurements. An indium tin oxide-coated glass substrate was cleaned with solvents and etched on one side. A thin layer of poly(3,4-ethylenedioxythiophene):polystyrenesulfonic acid (PEDOT:PSS, 1.4 wt % dispersion in water/isopropanol, viscosity 20 cps) was deposited using the doctor blade (DB, Sheen Instrument Model S265674) onto the ITO glass substrate and heated at 130 °C for 2 h at low pressure. A solution of 5 mg of COP (or PT10Br/PCBM 1:1 w/w) in 1 mL of CB was deposited by DB onto the PEDOT:PSS layer and heated in an oven at 120 °C for 0.5 h. Solar cells were then completed by evaporating a thin layer of aluminum on the top of the active layer using an Edwards vacuum coater (model 6306A). The fabricated cells had the following architecture: ITO (80 nm, anode)/PEDOT:PSS (100 nm; positive holes buffer layer)/photoactive layer (150 nm, COP or PT10Br/PCBM)/Al (50 nm, cathode) and a final active area of 0.0625 cm^2.

J−*V* characteristics of the devices were measured in air using a Keithley 2401 electrometer under simulated 100 mW cm^{-2} AM 1.5 solar irradiation provided by an Abet Technologies Solar Simulator model LS-150, which was previously calibrated using an ILT photometer model 1400-BL. External quantum efficiency (EQE) measurements were performed by means of an SCSpecIII (SevenStar Optics) solar cell spectral test system. Layer thicknesses were measured using a Film Thickness Probe FTPAdvances FTPadv-2 (Sentech GmbH, Germany) equipped with FTPExpert software.

Synthesis of 2,5-Dibromo-3-(10-bromodecyl)-thiophene (2,5BT10Br). 3-(10-Bromodecyl)thiophene (7.37 g, 24.3 mmol), prepared according to ref 48 was dissolved in 25 mL of anhydrous *N*,*N*-dimethylformamide (DMF), whereas 4.32 g (24.3 mmol) of *N*-bromosuccinimide (NBS) was dissolved in 25 mL of DMF and added dropwise. After stirring for 6 h at room temperature under an inert atmosphere in the dark, 6.48 g (36.4 mmol) of NBS in 36 mL of DMF was added. The mixture was reacted for 24 h, poured into 900 mL of distilled water, and then extracted several times with *n*-heptane (6 × 250 mL). The organic phases were collected, dried, and concentrated at reduced pressure, yielding 8.62 g (18.7 mmol) of the crude product. After purification by column chromatography (SiO_2/*n*-heptane), 7.53 g (67% yield) of pure 2,5BT10Br was obtained.

^{1}H NMR ($CDCl_3$, ppm): δ 6.76 (1H, s, *H4*Th); 3.41 (2H, t, CH_2Br); 2.54 (2H, t, ThCH_2); 1.88 (2H, m, CH_2), 1.66 (2H, m, CH_2), 1.44 (2H, m, CH_2), 1.35 (2H, m, CH_2), 1.31−1.24 (8H, m, CH_2).

^{13}C NMR ($CDCl_3$, ppm): δ 143.28 (ThC3), 131.61 (ThC4), 111.32 (ThC5), 109.43 (ThC2), 34.51 (CH_2Br), 33.46 (CH_2CH_2Br), 30.07 (CH_2Th), 29.62 (CH_2), 29.53 (CH_2), 29.31 (CH_2), 29.14 (CH_2), 28.88 (CH_2), 28.61 (CH_2), 28.47 (CH_2).

FT-IR (KBr, cm^{-1}): 3088, 2932, 2856, 1540, 1462, 1433, 1417, 1254, 1005, 827, 646, 472.

Synthesis of Poly[3-(10-bromodecyl)thiophene] (PT10Br). A total of 1.02 mL of a 3.0 M CH_3MgCl solution (3.06 mmol) in *n*-butyl ether was added to 1.41 g (3.06 mmol) of 2,5BT10Br in 25 mL of anhydrous THF. After refluxing for 2 h under argon while gently stirring, 8.29 mg (0.015 mmol) of [1,3-bis(diphenylphosphino)propane] nickel (II) chloride ($NiDPPPCl_2$) was added and the mixture was refluxed for 1 h. The crude polymer was recovered by the addition of 300 mL of methanol to the solution and subsequent filtration on a poly(tetrafluoroethylene) (PTFE) membrane (0.45 μm pore size), yielding 0.79 g of PT10Br (2.62 mmol, 86% yield). After fractionation by dissolution in 10 mL of methylene chloride and precipitation with 100 mL of methanol, 0.70 g (2.33 mmol, 76% yield) of a dark-red polymer was obtained.

^{1}H NMR ($CDCl_3$, ppm): δ 6.98 (1H, s, *H4*Th); 3.41 (2H, t, CH_2Br); 2.82 (2H, m, ThCH_2); 1.91−1.37 (16H, bm, CH_2).

^{13}C NMR ($CDCl_3$, ppm): δ 140.31 (ThC3), 134.87 (ThC5), 130.98 (ThC2), 128.81 (ThC4), 34.69 (CH_2Br), 33.56 (CH_2CH_2Br), 30.45 (CH_2Th), 29.88 (CH_2), 29.61 (CH_2), 29.17 (CH_2), 29.01 (CH_2), 28.76 (CH_2), 28.63 (CH_2), 28.35 (CH_2).

FT-IR (Ge, cm^{-1}): 3051, 2932, 2856, 1561, 1508, 1458, 1260, 1088, 830, 728, 644, 564, 523.

Elemental analysis: Calcd for $(C_{14}H_{21}BrS)_n$: C 55.81; H 7.03; Br 26.52; S 10.64; found: C 55.92; H 6.97; Br 26.38; S 10.73.

Synthesis of Poly[3-(10-bromodecyl)thiophene-*co*-3-(10-fullerenyldecyl)thiophene] (COP1). PT10Br (0.200 g, 0.664 mmol) in 10 mL of anhydrous THF was added dropwise to 2.43 mg (0.100 mmol) of Mg turnings under stirring and in an inert atmosphere. The mixture was refluxed for 20 h, cooled down to room temperature, and then transferred via a cannula to a solution of 0.072 g (0.100 mmol) of C_{60} fullerene in 300 mL of anhydrous toluene and 1.5 mL of anhydrous *N*,*N*-dimethylformamide (DMF). The reaction mixture was stirred for 90 min under an inert atmosphere and then 2.5 mL of a 1.87 M aqueous solution of NH_4Cl and 100 mL of brine were added. The organic phase was washed several times with distilled water, dried with $MgSO_4$, and concentrated. The recovered solid was exhaustively extracted in a Soxhlet apparatus, first with methanol and then with acetone, to remove the residual fullerene. The copolymer was then dissolved in 10 mL of $CHCl_3$, and the solution obtained was dropped into 150 mL of *n*-heptane. After filtration on a PTFE membrane (0.45 μm pore size), 0.190 g (0.511 mmol) of fractionated COP1 was obtained (77% yield).

^{1}H NMR ($CDCl_3$, ppm): δ 7.01 (s, H4 + H4′); 6.45 (s, H16′); 3.58 (m, H15′); 3.42 (m, H15); 2.83, 2.58 (m, H6 + H6′); 1.90−1.23 (3bm, H7 + H8 + H9 + H10 + H11 + H12 + H13 + H14 + H7′ + H8′ + H9′ + H10′ + H11′ + H12′ + H13′ + H14′).

^{13}C NMR ($CDCl_3$, ppm): δ 159.99 (C_{60}), 157.96 (C_{60}), 153.71 (C_{60}), 145.07 (C_{60}), 144.92 (C_{60}), 143.69 (C_{60}), 143.55 (C_{60}), 143.37 (C_{60}), 143.19 (C_{60}), 142.95 (C_{60}), 142.67 (C_{60}), 142.33 (C_{60}), 142.16 (C_{60}), 142.05 (C_{60}), 141.90 (C_{60}), 141.79 (C_{60}), 141. 66 (C_{60}), 141.11 (C_{60}), 140.06 (C_{60}), 139.21 (C3 + C3′), 137.77 (C_{60}), 137.54 (C_{60}), 137.39 (C_{60}), 136.82 (C_{60}), 136.36 (C_{60}), 136.13 (C_{60}), 134.53 (C_{60}), 133.95 (C5 + C5′), 129.71 (C2 + C2′), 127.93 (C4 + C4′), 126.96 (C_{60}), 125.18 (C_{60}), 124.87 (C_{60}), 122.82 (C_{60}), 61.34 (C15′), 42.55 (C14′), 34.68 (C15), 34.15 (C14), 31.24 (C6 + C6′), 30.81 (C13 + C13′), 30.35 (C7 + C7′), 29.99 (C8 + C8′), 29.56 (C12 + C12′), 29.03 (C9 + C9′), 28.38 (C10 + C10′ + C11 + C11′).

FT-IR (Ge, cm^{-1}): 3055, 2932, 2855, 1512, 1455, 1429, 1259, 1174, 1031, 835, 749, 644, 577, 563, 526.

Elemental analysis: Calcd for $[(C_{74}H_{22}S)_{0.11}(C_{14}H_{21}BrS)_{0.89}]$: C 66.53; H 5.72; Br 19.13; S 8.62; found: C 66.81; H 5.55; Br 18.95; S 8.69.

DOI: 10.1021/acsomega.9b02790
ACS Omega 2019, 4, 19863−19874

The same procedure was adopted for the synthesis of COP2, using 0.200 g (0.664 mmol) of PT10Br in 15 mL of anhydrous THF and 4.86 mg (0.200 mmol) of Mg turnings for the Grignard formation and 0.144 g (0.200 mmol) of C_{60} fullerene in 450 mL of anhydrous toluene and 2.0 mL of anhydrous *N*,*N*-dimethylformamide (DMF) for the coupling step. A total of 0.205 g (0.471 mmol) of fractionated COP2 was obtained (71% yield).

Elemental analysis: Calcd for $[(C_{74}H_{22}S)_{0.21}(C_{14}H_{21}BrS)_{0.79}]$: C 73.27; H 4.90; Br 14.48; S 7.35; found: C 73.83; H 4.67; Br 14.22; S 7.28.

COP3 was prepared following the procedure reported above. A total of 0.222 g (0.438 mmol) of fractionated COP3 was obtained (66% yield) starting from 0.200 g (0.664 mmol) of PT10Br in 20 mL of anhydrous THF and 7.26 mg (0.300 mmol) of Mg turnings for the Grignard formation and 0.216 g (0.300 mmol) of C_{60} fullerene in 600 mL of anhydrous toluene and 2.5 mL of anhydrous *N*,*N*-dimethylformamide (DMF) for the coupling step.

Elemental analysis: Calcd for $[(C_{74}H_{22}S)_{0.32}(C_{14}H_{21}BrS)_{0.68}]$: C 78.71; H 4.24; Br 10.72; S 6.33; found: C 78.92; H 4.16; Br 10.64; S 6.28.

NMR and FT-IR spectra of COP2 and COP3 showed the same signals reported for COP1.

■ ASSOCIATED CONTENT

Supporting Information

The Supporting Information is available free of charge on the ACS Publications website at DOI: 10.1021/acsomega.9b02790.

Synthesis of poly(3-decylthiophene) (PT10H); GPC eluograms of the examined polymers (intensity vs elution time); UV−vis absorption spectrum of PT10Br in a film; and efficiency of PT10H/PCBM cells heated at 150 °C over time (average PCE of four devices) (PDF)

■ AUTHOR INFORMATION

Corresponding Author

*E-mail: massimiliano.lanzi@unibo.it.

ORCID

Massimiliano Lanzi: 0000-0002-2466-2813

Filippo Pierini: 0000-0002-6526-4141

Notes

The authors declare no competing financial interest.

■ ACKNOWLEDGMENTS

This study was partially supported by the First TEAM grant number POIR.04.04.00-00-5ED7/18-00, which is carried out within the framework of the First TEAM programme of the Foundation for Polish Science (FNP), co-financed by the European Union under the European Regional Development Fund. The authors are also grateful for the support of this work by the Canaletto programme (grant number PPN/BIL/2018/2/00035/U/00001), funded by the National Agency for Academic Exchange (NAWA) and the Italian Ministero degli Affari Esteri e della Cooperazione Internazionale (Farnesina), Project PO19MO13.

■ ABBREVIATIONS

OSC,organic solar cell; PCE,power conversion efficiency; BHJ,bulk heterojunction; 2,5BT10Br,2,5-dibromo-3-(10-bromodecyl)thiophene; PT10Br,poly[3-(10-bromodecyl)-thiophene]; COP,poly[3-(10-bromodecyl)thiophene-*co*-3-(10-fullerenyldecyl)thiophene]; CB,chlorobenzene; THF,tetrahydrofuran; DMF,*N*,*N*-dimethylformamide; NBS,*N*-bromosuccinimide; NiDPPPCl$_2$,[1,3-bis(diphenylphosphino)propane] nickel (II) chloride; GRIM,Grignard metathesis; HT,head-to-tail; TT,tail-to-tail; HH,head-to-head; FT-IR,Fourier transform infrared; GPC,gel permeation chromatography; M_n,number-average molecular weight; M_w,weight-average molecular weight; M_w/M_n,polydispersity index; ITO,indium tin oxide; PEDOT:PSS,poly(3,4-ethylenedioxythiophene):polystyrenesulfonic acid; Al,aluminum; TGA,thermogravimetric analysis; SEM,scanning electron microscopy; AFM,atomic force microscopy; DSC,differential scanning calorimetry; T_g,glass-transition temperature; T_m,melting temperature; T_c,crystallization temperature; T_d,decomposition temperature; XRD,X-ray diffraction; UV−vis,ultraviolet−visible; P3HT,regioregular poly(3-hexylthiophene); PCBM,[6,6]-phenyl C_{61}-butyric acid methyl ester; TBAPF$_6$,tetrabutylammonium hexafluorophosphate; $E_{g,ec}$,electrochemical band gap; $E_{g,opt}$,optical band gap; E_{ox},oxidation potential; E_{HOMO},HOMO orbital level energy; E_{LUMO},LUMO orbital level energy; EQE,external quantum efficiency; *J*−*V*,current density versus voltage; AM,air mass; J_{sc},short-circuit current density; V_{oc},open-circuit voltage; FF,fill factor; PCE,power conversion efficiency

■ REFERENCES

(1) Murali, M. G.; Rao, A. D.; Yadav, S.; Ramamurthy, P. C. Narrow band gap conjugated polymer for improving the photovoltaic performance of P3HT: PCBM ternary blend bulk heterojunction solar cells. *Polym. Chem.* **2015**, *6*, 962−972.

(2) Swager, T. M. 50th Anniversary Perspective: Conducting/Semiconducting Conjugated Polymers. A Personal Perspective on the Past and the Future. *Macromolecules* **2017**, *50*, 4867−4886.

(3) Berger, P. R.; Kim, M. Polymer solar cells: P3HT: PCBM and beyond. *J. Renewable Sustainable Energy* **2018**, *10*, No. 013508.

(4) Dang, M. T.; Hirsch, L.; Wantz, G. P3HT: PCBM, best seller in polymer photovoltaic research. *Adv. Mater.* **2011**, *23*, 3597−3602.

(5) Schilinsky, P.; Waldauf, C.; Brabec, C. J. Recombination and loss analysis in polythiophene based bulk heterojunction photodetectors. *Appl. Phys. Lett.* **2002**, *81*, 3885−3887.

(6) Li, G.; Shrotiya, V.; Yao, Y.; Yang, Y. Investigation of annealing effects and film thickness dependence of polymer solar cells based on poly (3-hexylthiophene). *J. Appl. Phys.* **2005**, *98*, No. 043704.

(7) Mikhnenko, O. V.; Blom, P. W. M.; Nguyen, T. G. Exciton diffusion in organic semiconductors. *Energy Environ. Sci.* **2015**, *8*, 1867−1888.

(8) Erb, T.; Zhoukhavets, U.; Gobsch, G.; Raleva, S.; Stuehn, B.; Schilinsky, P.; Waldauf, C.; Brabec, C. J. Correlation between structural and optical properties of composite polymer/fullerene films for organic solar cells. *Adv. Funct. Mater.* **2005**, *15*, 1193−1196.

(9) Savagatrup, S.; Makaram, A. S.; Burke, D. J.; Lipomi, D. J. Mechanical properties of conjugated polymers and polymer-fullerene composites as a function of molecular structure. *Adv. Funct. Mater.* **2014**, *24*, 1169−1181.

(10) Mei, J.; Bao, Z. Side chain engineering in solution-processable conjugated polymers. *Chem. Mater.* **2014**, *26*, 604−615.

(11) Miyanishi, S.; Zhang, Y.; Hashimoto, K.; Tajima, K. Controlled synthesis of fullerene-attached poly (3-alkylthiophene)-based copolymers for rational morphological design in polymer photovoltaic devices. *Macromolecules* **2012**, *45*, 6424−6437.

(12) Zhang, F.; Svensson, M.; Andersson, M. R.; Maggini, M.; Bucella, S.; Menna, E.; Inganas, O. Soluble polythiophenes with pendant fullerene groups as double cable materials for photodiodes. *Adv. Mater* **2001**, *13*, 1871−1874.

DOI: 10.1021/acsomega.9b02790
ACS Omega 2019, 4, 19863−19874

(13) Liang, S.; Xu, Y.; Li, C.; Li, J.; Wang, D.; Li, W. Realizing Lamellar Nanophase Separation in a Double-Cable Conjugated Polymer via Solvent Annealing Process. *Polym. Chem.* **2019**, *10*, 4584−4592.
(14) Yang, F.; Li, J.; Li, C.; Li, W. Improving Electron Transport in a Double-Cable Conjugated Polymer via Parallel Perylenetriimide Design. *Macromolecules* **2019**, *52*, 3689−3696.
(15) Lai, W.; Li, C.; Zhang, J.; Yang, F.; Colberts, F. J. M.; Guo, B.; Wang, Q. M.; Li, M.; Zhang, A.; Janssen, R. A. J.; Zhang, M.; Li, W. Diketopyrrolopyrrole-based conjugated polymers with perylene bisimide side chains for single-component organic solar cells. *Chem. Mater.* **2017**, *29*, 7073−7077.
(16) Van Hal, P.; Beckers, E. H. A.; Meskers, S. C. J.; Janssen, R. A. J.; Jousselme, B.; Blanchard, P.; Roncali, J. Orientational Effect on the Photophysical Properties of Quaterthiophene−C60 Dyads. *Chem. - Eur. J.* **2002**, *8*, 5415−5429.
(17) Feng, G.; Li, J.; He, Y.; Zheng, W.; Wang, J.; Li, C.; Tang, Z.; Osvet, A.; Li, N.; Brabec, C. J.; Yi, Y.; Yan, H.; Li, W. Thermal-driven phase separation of double-cable polymers enables efficient single-component organic solar cells. *Joule* **2019**, *3*, 1765−1781.
(18) Li, M. H.; Xu, P.; Yang, J. G.; Yang, S. F. J. Donor-π-acceptor double-cable polythiophenes bearing fullerene pendant with tunable donor/acceptor ratio: A facile postpolymerization. *J. Mater. Chem.* **2010**, *20*, 3953−3960.
(19) Matsuo, Y.; Iwashita, A.; Abe, Y.; Li, C. Z.; Matsuo, K.; Hashiguchi, M.; Nakamura, E. Regioselective synthesis of 1,4-di(organo)[60]fullerenes through DMF-assisted monoaddition of silylmethyl Grignard reagents and subsequent alkylation reaction. *J. Am. Chem. Soc.* **2008**, *130*, 15429−15436.
(20) Lanzi, M.; Salatelli, E.; Benelli, T.; Caretti, D.; Giorgini, L.; Di-Nicola, F. P. A regioregular polythiophene−fullerene for polymeric solar cells. *J. Appl. Polym. Sci.* **2015**, *132*, No. 42121.
(21) Parenti, F.; Tassinari, F.; Libertini, E.; Lanzi, M.; Mucci, A. π-Stacking signature in NMR solution spectra of thiophene-based conjugated polymers. *ACS Omega* **2017**, *2*, 5775−5784.
(22) Loewe, R. S.; Ewbank, P. C.; Liu, J.; Zhai, L.; McCullough, R. D. Regioregular, head-to-tail coupled poly (3-alkylthiophenes) made easy by the GRIM method: Investigation of the reaction and the origin of regioselectivity. *Macromolecules* **2001**, *34*, 4324−4333.
(23) Miyanishi, S.; Tajima, K.; Hashimoto, K. Morphological stabilization of polymer photovoltaic cells by using cross-linkable poly (3-(5-hexenyl) thiophene. *Macromolecules* **2009**, *42*, 1610−1618.
(24) Chirvase, D.; Parisi, J.; Hummelen, J. C.; Dyanokov, V. Influence of nanomorphology on the photovoltaic action of polymer−fullerene composites. *Nanotechnology* **2004**, *15*, 1317−1323.
(25) Boudouris, B. W.; Molins, F.; Blank, D. A.; Frisbie, C. D.; Hillmyer, M. A. Synthesis, optical properties, and microstructure of a fullerene-terminated poly (3-hexylthiophene). *Macromolecules* **2009**, *42*, 4118−4126.
(26) Qian, R. Aspects of molecular design of conducting polymers. *Makromol. Chem., Macromol. Symp.* **1990**, *33*, 327−339.
(27) Jiang, M. Q. *Rule of Homologous Linearity of Organic Compounds*; Science Press: Beijing, 1980; p 184.
(28) Clark, J.; Silva, C.; Friend, R. H.; Spano, F. C. Role of intermolecular coupling in the photophysics of disordered organic semiconductors: aggregate emission in regioregular polythiophene. *Phys. Rev. Lett.* **2007**, *98*, No. 206406.
(29) Murali, M. G.; Rao, A. D.; Yadav, S.; Ramamurthy, P. C. Narrow band gap conjugated polymer for improving the photovoltaic performance of P3HT: PCBM ternary blend bulk heterojunction solar cells. *Polym. Chem.* **2015**, *6*, 962−972.
(30) Pommerehne, J.; Westweber, H.; Guss, W.; Mahrt, R. F.; Bassler, H.; Porsch, M.; Daub, J. Efficient two layer leds on a polymer blend basis. *Adv. Mater.* **1995**, *7*, 551−554.
(31) Bredas, J. L. Mind the gap! *Mater. Horiz.* **2014**, *1*, 17−19.
(32) Haufler, R. E.; Conceicao, J.; Chibante, L. P. F.; Chai, Y.; Byrne, N. E.; Flanagan, S.; Haley, M. M.; O'Brien, S. C.; Pan, B. C.; Xiao, Z.; Billups, W. E.; Ciufolini, M. A.; Hauge, R. H.; Margrave, J. L.; Wilson, L. J.; Curl, R. F.; Smalley, R. E. Efficient production of C_{60} (buckminsterfullerene), $C_{60}H_{36}$, and the solvated buckide ion. *J. Phys. Chem. A* **1990**, *94*, 8634−8636.
(33) Lanzi, M.; Di Nicola, F. P.; Errani, F.; Paganin, L.; Mucci, A. Solventless deposition of oligo-and polythiophenes for bulk heterojunction solar cells. *Synth. Met.* **2014**, *195*, 61−68.
(34) Richter, T. V.; Braun, C. H.; Link, S.; Scheuble, M.; Crossland, E. J. W.; Stelzl, F.; Wuerfel, U.; Ludwigs, S. Regioregular polythiophenes with alkylthiophene side chains. *Macromolecules* **2012**, *45*, 5782−5788.
(35) Scharber, M. C.; Muehlbacher, D.; Koppe, M.; Denk, P.; Waldauf, C.; Heeger, A. J.; Brabec, C. J. Design rules for donors in bulk-heterojunction solar cells—Towards 10% energy-conversion efficiency. *Adv. Mater.* **2006**, *18*, 789−794.
(36) Schilinsky, P.; Waldauf, C.; Hauch, J.; Brabec, C. J. Simulation of light intensity dependent current characteristics of polymer solar cells. *J. Appl. Phys.* **2004**, *95*, 2816.
(37) Tashiro, K.; Ono, K.; Minagawa, Y.; Kobayashi, M.; Kawai, T.; Yoshino, K. Structure and thermochromic solid-state phase transition of poly (3-alkylthiophene). *J. Polym. Sci., Part B: Polym. Phys.* **1991**, *29*, 1223−1233.
(38) Malik, S.; Nandi, A. K. Crystallization mechanism of regioregular poly(3-alkylthiophene)s. *J. Polym. Sci., Part B: Polym. Phys.* **2002**, *40*, 2073−2085.
(39) Kumar, J.; Singh, R. K.; Kumar, V.; Rastogi, R. C.; Singh, R. Self-assembly of SWCNT in P3HT matrix. *Diamond Relat. Mater.* **2007**, *16*, 446−453.
(40) Kim, H.; Shin, M.; Kim, Y. Distinct annealing temperature in polymer: fullerene: polymer ternary blend solar cells. *J. Phys. Chem. C* **2009**, *113*, 1620−1623.
(41) Pierini, F.; Lanzi, M.; Nakielski, P.; Pawłowska, S.; Urbanek, O.; Zembrzycki, K.; Kowalewski, T. A. Single-Material Organic Solar Cells Based on Electrospun Fullerene-Grafted Polythiophene Nanofibers. *Macromolecules* **2017**, *50*, 4972−4981.
(42) Choulis, S. A.; Nelson, J.; Kim, Y.; Poplavskyy, D.; Kreouzis, T.; Durrant, J. R.; Bradley, D. D. C. Investigation of transport properties in polymer/fullerene blends using time-of-flight photocurrent measurements. *Appl. Phys. Lett.* **2003**, *83*, 3812−3814.
(43) Li, Y.; Huang, W.; Huang, H.; Hewitt, C.; Chen, Y.; Fang, G.; Carroll, D. L. Evaluation of methods to extract parameters from current−voltage characteristics of solar cells. *Solar Energy* **2013**, *90*, 51−57.
(44) Padinger, F.; Rittberger, R. S.; Sariciftci, N. S. Effects of postproduction treatment on plastic solar cells. *Adv. Funct. Mater.* **2003**, *13*, 85−88.
(45) Mihailetchi, V. D.; Xie, H.; de Boer, B.; Koster, L. J. A.; Blom, P. W. M. Charge transport and photocurrent generation in poly (3-hexylthiophene):methanofullerene bulk-heterojunction solar cells. *Adv. Funct. Mater.* **2006**, *16*, 699−708.
(46) Lee, K. S.; Yeon, K. Y.; Jung, K. H.; Kim, S. K. Direct Observation of the Primary and Secondary C−Br Bond Cleavages from the 1,2-Dibromopropane Photodissociation at 234 and 265 nm Using the Velocity Map Ion Imaging Technique. *J. Phys. Chem. A* **2008**, *112*, 9312−9317.
(47) Tang, Y.; Ji, L.; Zhu, R. S.; Wei, Z. R.; Zhang, B. Photodissociation study of 1,3-dibromopropane at 234 nm via an ion velocity imaging technique. *J. Phys. Chem. A* **2005**, *109*, 11123−11126.
(48) Bäuerle, P.; Wurtner, F.; Heid, S. Facile Synthesis of 3-(ω-Haloalkyl) thiophenes as Key Building Blocks for Functionalized Thiophenes and Polythiophenes. *Angew. Chem., Int. Ed.* **1990**, *29*, 419−420.

DOI: 10.1021/acsomega.9b02790
ACS Omega 2019, 4, 19863−19874